Physica Scripta

PAPER

n-type SnS_2 thin films spray-coated from transparent molecular ink as a non-toxic buffer layer for solar photovoltaics

RECEIVED
25 May 2022

REVISED
2 August 2022

ACCEPTED FOR PUBLICATION
5 August 2022

PUBLISHED
18 August 2022

Sabrina Tair[1], Prashant R Ghediya[2,8,*], Abdelkader Nebatti Ech-Chergui[1,3,*], M'hamed Guezzoul[4], Sanat Kumar Mukherjee[5], Kouider Driss-Khodja[6], Rajan Singh[5], Jaymin Ray[7] and Bouhalouane Amrani[6]

[1] Faculty of Sciences and Technology, University Belhadj Bouchaib, BP 284, 46000 Ain-Temouchent, Algeria
[2] Department of Physics, Marwadi University, Rajkot, Gujarat 360003, India
[3] Laboratory of Materials Sciences and Applications (LMSA) University of Ain-Temouchent Belhadj Bouchaib, Algeria
[4] Laboratory of materials (LABMAT), National Polytechnique School (ENP) of Oran, BP 1523 Oran Mnaouar, Oran, Algeria
[5] Department of Physics, Birla Institute of Technology, Mesra, Ranchi—835215, India
[6] Laboratoire De Théorie et Simulation Des Matériaux, Université Oran1 Ahmed Ben Bella, Oran, Algerie
[7] Department of Physics, UKA Tarsadia University, Maliba Campus, Bardoli-Mahuva Road, Bardoli—394350, Dist—Surat, Gujarat, India
[8] **Present address:** Research Institute for Electronic Science, Hokkaido University, N20W10, Kita, Sapporo 001-0020, Japan.
[*] Authors to whom any correspondence should be addressed.

E-mail: prashantghediya@gmail.com **and** abdelkader.nebatti@daad-alumni.de

Keywords: SnS_2, spray-coating, transparent molecular ink, thin films, x-ray photoelectron spectroscopy

Abstract

This paper reports the effect of solvent evaporation temperature on spray-coated tin disulfide (SnS_2) thin films from molecular ink. Thiourea and tin chloride were the key chemical reagents used for the synthesis of SnS_2 transparent ink under atmospheric conditions. The structural and compositional properties of SnS_2 thin films revealed formation of pristine hexagonal SnS_2. The films are smooth, homogeneous resulting in band gaps ranging from 2 to 2.22 eV suited for a Cd-free alternative buffer layer for Cu-based multicomponent solar cells. Thermoelectric power measurement showed that tin disulfide films exhibit n-type conductivity. Activation energy estimated from temperature variation of electrical conductivity measurement varied from 40 to 90 mV. Our results suggest that ink-processed SnS_2 can be used as a potential alternative for opto-electronic devices such as thin film solar cell and photodetector devices.

1. Introduction

In view of the possibility of replacing the traditional and toxic CdS layer for various Cu-based multicomponent chalcogenide thin film solar cells (TFSCs) such as $Cu(In,Ga)Se_2$ (CIGS), Cu_2ZnSnS_4 (CZTS), Cu_2SnS_3 (CTS), Cu_2NiSnS_4 (CNTS), Cu_2CoSnS_4 (CCoTS), etc, earth abundant non-toxic, low-cost tin disulfide (SnS_2) is emerged as a potential alternative buffer layer due to its favourable opto-electronic properties [1, 2]. It is a binary inorganic semiconductor compound with hexagonal cadmium iodide (CdI2) type structure. Additionally, their simple composition and promising physical properties made them suitable candidates for applications such as photocatalytic, thermoelectric, and has been explored as an alternate buffer layer for p-CIGS/CZTS thin film solar cells [3–6]. However, quaternary absorbers such as CIGS/CZTS often need to be annealed at high temperature (500 °C under Ar) for grain growth which eventually limits the production of superstrate-type solar cells. It is well known that in superstrate (reverse) type solar cells, the absorber layer is coated after the n-type buffer layer [6]. Hence, it is therefore necessary to deposit n-type thin films at relatively low temperatures (<300 °C) to form a proper junction.

Until now, several techniques have been employed to produce SnS_2 thin films. However, direct coating methods [7, 8] such as spin-coating, drop-casting, spray-coating, etc, have the capabilities to bring down the overall costs due to their high material usage and amenability to large scale. Amongst them, the chemical spray pyrolysis is particularly simple, non-vacuum system and truly scalable that can be useful for cost-effective large

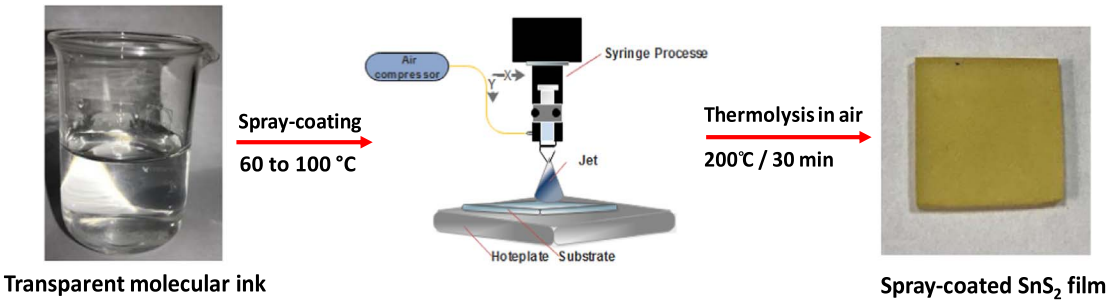

Figure 1. Spray-coating of SnS_2 films from transperent molecular ink.

area synthesis in the industrial production of optoelectronic devices [9, 10]. Fine-tuning of the experimental parameters during the spray process can produce high quality films and devices.

In general, a spray system has two options : spray-coating (SC) and spray pyrolysis (SP).

In the SnS_2 system, mostly the thin films have been deposited by spray pyrolysis (SP) technique [11–13] while there is no report on spray-coating of SnS_2 thin films. In the SP process, the precursor layer is composed of inorganic salts or organometallic compounds dissolved in aqueous molecular ink directly annealed at higher temperature (300 to 400 °C) to achieve phase purity of the semiconductor thin films. However, in case of SC, the films were first heated at low substrate temperature depending upon the boiling point of the solvent used for development of inks. Films will be then thermolyzed at 200 to 300 °C temperature followed by annealing at high temperature (500 °C) for the formation of compact grains under Ar or N2 atmosphere. Since the preheating temperature of the substrates required in the spray-pyrolysis is quite high (>300 °C), thin film deposition by this process resulted in porosity and/or cracks. Thin film formation by SC leads to smooth, shiny and homogenous microstructure due to low substrate temperature [14].

SC is a versatile ink-based low-temperature technique that has been broadly used to deposit thin films of organic materials for solar cells, OLEDs, carbon nanotubes, etc. In this paper, we report for the first-time spray-coating of inorganic SnS_2 thin films from transparent molecular ink developed with methanol. Thin films were first sprayed at extremely low temperature (from 60 to 100 °C) followed by annealed at 200 °C in air for 30 min Raman spectroscopy confirms the formation of pristine hexagonal SnS_2. The films are n-type and show band gap energy varied from 2 to 2.22 eV. Films are smooth, homogeneous and compact having an activation energy varied from 40 to 90 meV depending upon solvent evaporation température. Our investigation paves the way for ink-processed SnS_2 thin films as a potential buffer layer for solar cells.

2. Experimental

SnS_2 molecular ink was synthesised in a similar manner as described elsewhere for CZTS [15], CTS [16] and CCoTS [17]. Tin chloride and thiourea were chosen as a starting precursor, while methanol was used as a solvent. The 0.05 M tin chloride and 0.1 M of thiourea were dissolved in 20 ml methanol. Few drops of HCL were added into the above mixture to prevent hydrolysis of $SnCl_2$. The obtained solution was then stirred for 30 min in a magnetic stirrer resulting in a transparent ink as depicted in figure 1.

A spray machine (HO-TH-04, Holmarc Ltd, India) based on syringe pump spray-coating (SPSC) method is used for the deposition of SnS2 films. The system has an ultrasonic spray head with software-controlled X-Y movements. The nozzle's vertical distance from the sample is kept fixed. 20 ml of ink was taken into a glass syringe pump and injected through a spray nozzle. The inner diameter of the nozzle is 0.2 mm [18]. To attain the appropriate droplet sizes, a carrier gas with regulated airflow was used. Cleaned glass substrates (20 mm × 10 mm) were placed on a hot plate and heated to a desired temperature for solvent evaporation. After being thoroughly cleaned, the glass substrates were placed on a hot plate and heated to the desired temperature for solvent evaporation. The substrates were placed 13 cm away from the syringe. The syringe was directly sprayed as fine droplets onto the preheated substrates for 3 min. The pressure of the carrier gas was kept constant at 1 bar during the deposition process. The dispensing spray rate was kept fixed at 500 μlmin^{-1}. The substrate temperature of spray-coated films was varied from 60 to 100 °C to see the effect of solvent evaporation temperatures on physical properties of the films. The precursor films were gradually converted into pale yellow films (figure 1) by heating at 200 °C in air for 30 min. Finally, three different types of SnS_2 thin films were characterized for their structural and compositional, optical, morphological, and electrical properties: S1 °C–60 °C, S2 °C–80 °C and S3 °C–100 °C.

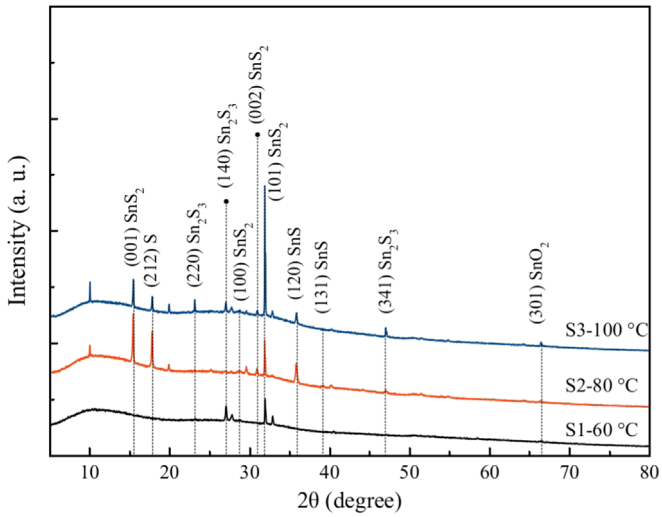

Figure 2. X-ray diffraction of spray-coated SnS_2 thin films.

2.1. Characterizations

The compositional properties were determined by x-ray diffractometer (XRD, SmartLab 9 kW, Rigaku, Japan) with Ni-filtered CuKa radiation ($\lambda = 1.5418$ Å) operated in the 2Θ range from 10 to 80°. The vibration modes of SnS_2 thin films were studied by a confocal micro-Raman spectrometer (AIRIX Corp., STR500) with a laser excitation wavelength of 532 nm Ar + laser. The transmittance spectra were obtained by UV–vis-NIR spectrophotometer (Perkin Elmer, LAMBDA750) in the wavelength range of 300 to 1300 nm. Scanning electron microscope (SEM, JSM 6390 LV, Jeol, Japan) fitted with EDX was used to observe the surface morphology and elemental composition of thin films. X-ray photoelectron spectroscopy (XPS) analysis was performed in a Multiprobe XPS UHV-system of Scientaomicron using a dual-anode (Mg/Al) X-ray source 'Omicron DAR 400'. Here, the $Mg - K\alpha$ ($h\nu = 1253.6$ eV) energy line was adopted for excitation with a power source of 225 W corresponding to 15 kV and 15 mA of cathode voltage and emission current, respectively. All XPS spectra were recorded using the Argus hemispherical detector of 128 channels performing in Constant Analyzer Energy mode (CAE) with a pass energy of 50 eV. Due to the charge effect, the binding energies of XPS spectra are referenced to C 1 s line at 285 eV. To investigate the chemical composition, the atomic percentages (at%) of elements were calculated through the survey spectrum using CasaXPS software. The electrical properties were studied by conventional two-probe method/hot probe method.

3. Results and discussion

3.1. Structural and compositional properties

Figure 2 shows the x-ray diffraction (XRD) patterns of spray-coated SnS_2 thin films deposited from ink at different solvent temperatures (60 °C, 80 °C, 100 °C). It is observed that the films are grown in different phases SnS_2, Sn_2S_3, SnS, SnO_2 and S. Diffraction peaks at 15.53°, 28.82°, 30.98° and 32.03° corresponds to (001), (100), (002) and (101) plane of SnS_2 hexagonal structure (JCPDS Card No. 23-0677), respectively, with preferred orientation along (101) plane [12, 19]. The diffraction peaks observed at 23.17°, 27.04° and 47.07° corresponds to (220), (140) and (341) plane of Sn_2S_3 orthorhombic structure (JCPDS Card No. 14-0619), respectively [20, 21]. Peaks at 35.94° (120) and 39.25° (131) are related to SnS while peaks at 17.87° and 66.53° are related to S (212) and SnO_2 (301), respectively.

With increase in solvent evaporation temperatures, the number of peaks related to different phases of SnS_2 increases along with the intensity. However, it should be noted that reflections from the crystallographic planes (001), and (101) of the hexagonal phase of SnS_2 had the strongest intensity, while the intensity of peaks due to other phases were very weak. Furthermore, EDS elemental composition of spray-coated SnS_2 films revealed that the films are mainly composed of S, Sn as shown in table 1. No other peak related to impurity was detected from the elemental composition.

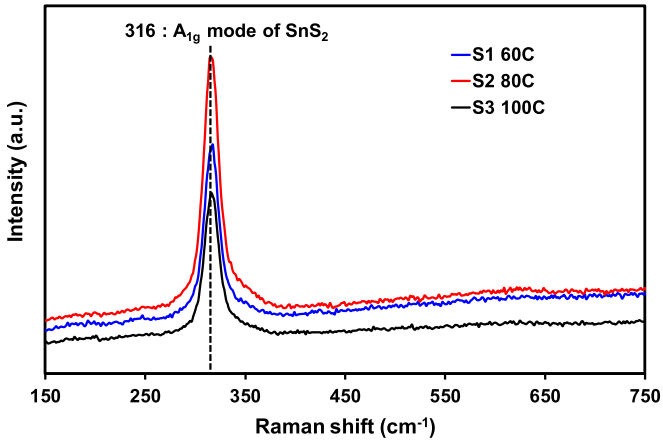

Figure 3. Raman spectra of spray-coated SnS_2 thin films.

Table 1. EDS elemental composition (Atomic Wt%) of spray-coated SnS_2 films.

Sample	Sn%	S%
S1 °C–60 °C	33.83	66.17
S2 °C–80 °C	37.26	62.74
S3 °C–100 °C	36.35	63.65

Table 2. Calculated values of the structural parameters of spray-coated SnS_2 thin films.

	Lattice constants (Å)					
Sample	a	c	c/a	Crystallite size (nm)	Strain (ε) ($\times 10^{-4}$)	Dislocation density (δ) ($\times 10^{-3}$ line/m^2)
S1–60C	3.577	5.783	1.617	50.3	5.72	39.5
S2–80C	3.567	5.776	1.619	57.4	3.14	30.3
S3–100C	3.575	5.770	1.614	78.3	2.76	16.3

The average crystallite size of SnS_2 thin films is calculated using Debye–Scherrer formula [22]:

$$D = \frac{0.9 \cdot \lambda}{\beta \cdot \ \mathrm{Cos}\ \theta} \tag{1}$$

Lattice strain is calculated using relation [23] :

$$\varepsilon = \frac{\beta \cdot \ \mathrm{Cos}\ \theta}{4} \tag{2}$$

and dislocation density using relation [24]:

$$\delta = \frac{1}{D^2} \tag{3}$$

Table 2 presents lattice constants (*a* & *c*), crystallite size, strain and dislocation density of SnS_2 films prepared at various solvent temperatures. Crystallite size of SnS_2 films range between 50—80 nm. An increasing trend in crystallite size is observed with increasing solvent temperature. Lattice strain and dislocation density shows decreasing trend with increasing crystallite size.

Due to XRD patterns similarities for the three known stoichiometric SnS, SnS_2 and Sn_2S_3, utilizing diffraction analysis alone to distinguish one stoichiometric from another is challenging. Raman spectroscopy is often used to overcome this constraint. The SnS_2 adopts a hexagonal structure with P3ml space group, similar to the structure of the CdI_2 system. Figure 3 shows the Raman spectra of the spray-coated SnS_2 thin films (S1 to S3). The Raman spectra reveal only sharp and intense peat at 316 cm^{-1}. According to theoretical [25] and experimental works [25–27], a peak appearing at 316 cm^{-1} is related to the A_{1g} vibrational mode of hexagonal

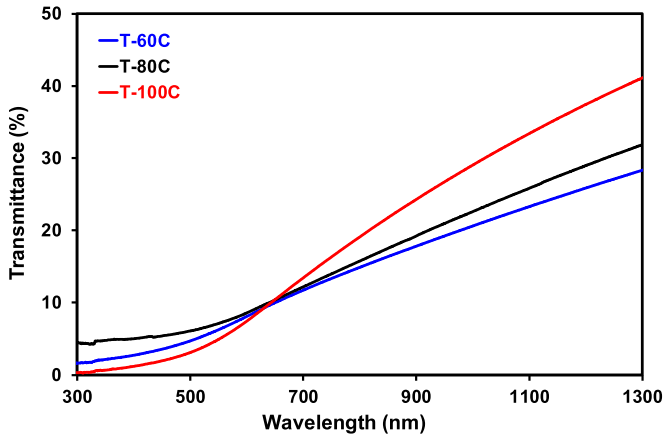

Figure 4. Transmittance spectra of SnS_2 thin films spray-coated from transparent molecular ink.

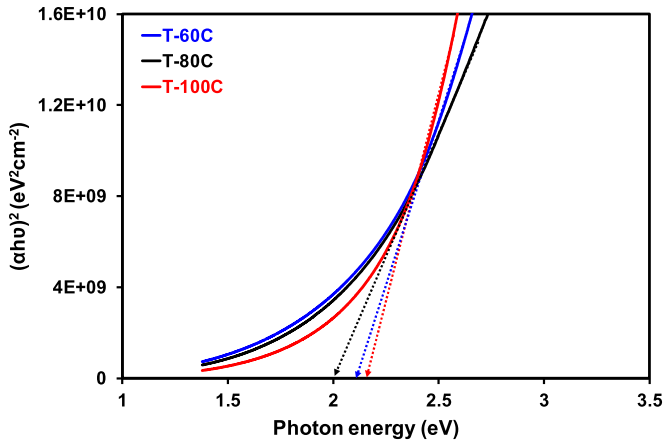

Figure 5. Tauc plot revealing band gap of SnS_2 thin films.

SnS_2 [21]. Peaks due to the other secondary phases of oxides or sulphides were absent confirmed formation of hexagonal SnS_2.

3.2. Bandgap measurement

Figure 4 shows the transmittance spectra of the spray-coated pristine SnS_2 thin films. Clearly, the transmittance (T) of films decreases with decreasing wavelength from 1300 to 300 nm. Furthermore, as the solvent evaporation temperature rises, the T of the films rises as well. The abrupt fall in T below 600 nm indicates an absorption edge caused by pristine SnS_2. However, the band edges slightly shift towards lower wavelengths, causing a shift change in band gaps, with an increment in solvent evaporation temperature.

The direct band gap of spray-coated SnS_2 thin films was determined using the well-known Tauc plot [28] as shown in figure 5. The band gap energy (Eg) is estimated by extrapolating the linear portion of the spectrum to zero. It can be observed that the Eg slightly changes from 2.2 to 2 eV with increasing solvent evaporation temperature. The obtained values of the Eg is nearer to the reported ones [29].

3.3. Surface morphology

Figure 6 shows the surface morphology of spray-coated SnS_2 thin film on glass as observed by scanning electron microscope. The films are dense and compact but some voids are visible on the surface. The polcryrstalline SnS_2 films consist of closely-packed interconnected grains. It can be seen that grains in the films improve with solvent evaporation temperature suggesting improvement in the crystallinity. The film thickness is estimated from the cross-sectional SEM. Depending upon the solvent evaporation temperatures, the film thickness is varied from ~7 to 14 μm.

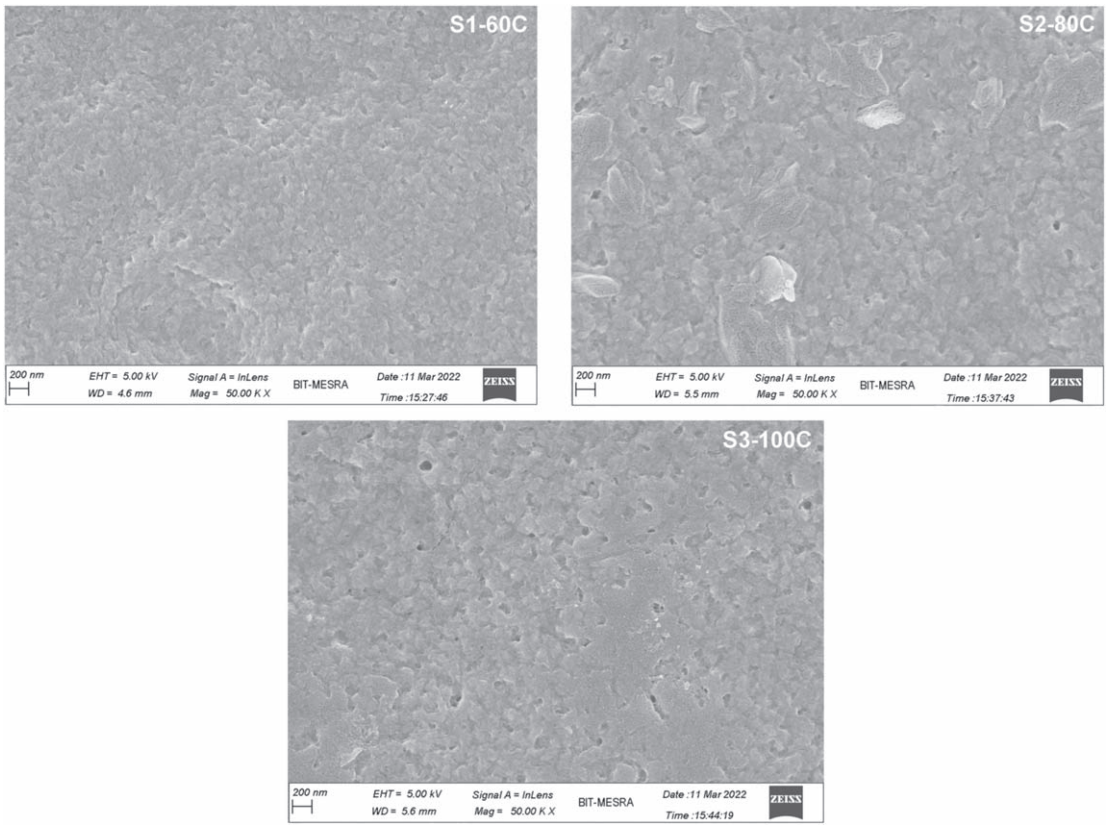

Figure 6. Scanning electron microscopy images of spray-coated SnS_2 thin films (60 to 100 °C).

3.4. Elemental composition and chemical state

Since no secondary phases apart from SnS_2 were found from structural, morphological and bandgap analysis, XPS of only final SnS_2 thin film (S3 °C–100 °C) is studied. Figure 7(a) displays the XPS survey spectrum, and the atomic percentages of elements presented in the spray-coated SnS_2 thin film. The core-level photoelectron peaks (Sn3p, Sn3d, Sn4d, S1s, S2s, and S2p) and Auger transition peaks (Sn MNN and S LMM) related to SnS_2 compound are well identified. In addition, four photoelectron peaks of N1s, C1s, O1s, and Cl 2p corresponding to the nitrogen, carbon, oxygen, and chloride elements, respectively, appear at the SnS_2 surface due to the starting precursors and/or ambient contaminant species. As shown in the inset table, despite the presence of the contamination layer that is dominated by carbon and nitrogen (>50%), the ratio of [Sn] to [S] is 0.55, which is close to the stoichiometric ratio of pure SnS_2. Figure 7(b) depicts the high-resolution XPS spectrum of Sn 3d doublet ($Sn3d_{5/2}$-$Sn3d_{3/2}$) submitted to Gaussian fitting combined with Shirley background subtraction. The later can be deconvoluted into three pairs of ($Sn3d_{5/2}$, $Sn3d_{3/2}$) sub-peaks with respecting their spin–orbit splitting (~8.4 eV) [30, 31] as follow: (i) a main pair at (486.9 eV, 495.3 eV) with a dominate area ratio (78.70%) attributed to Sn atoms in the Sn^{4+} valence state of Sn-S_2 bonds, (ii) the second pair is at low B.E (485.5 eV, 494.0 eV) and ascribed the Sn^{2+} valence state of Sn-S bonds, (iii) the third one is at high B.E (488.2 eV, 496.6 eV) and can be attributed to the Sn^{4+} valence state of Sn-O_2 bonds.

Similarly, figure 7(c) shows the deconvoluted high-resolution XPS spectrum assigned to the S2p core level peak. The S2p peak can be fitted into two pairs of ($S2p_{3/2}$, $S2p_{1/2}$) peaks by respecting their spin orbital splitting (1.16 eV) [30] as follows: the main pair (82.82%) at (161.68 eV, 162.84 eV) is attributed S-Sn bonds [32], whereas the second one (163.34 eV–164.5 eV) reflects a the small amount of S-C and S-O bonds [33, 34]. Finally, the Sn LMM Auger spectra also matches well with literature, showing a main peak at a banding energy of 832 eV, which would indicate the presence of metallic Sn.

3.5. Electrical properties

Electrical properties of SnS_2 thin films were measured at 300 K as tabularized in table 3. The negative sign in thermoelectric power (TEP) measurement reveals that the films are n-type. The electrical conductivity (σ in S/cm), TEP (μV/K), carrier concentration (n in cm^{-3}), and mobility (μ in cm^2/Vs) of different types of SnS_2 thin films were measured in a similar manner as reported earlier for Cu-based multicomponent thin films [15, 35]. Table 3 revealed that the electrical conductivity increases while TEP and carrier concentration decreases

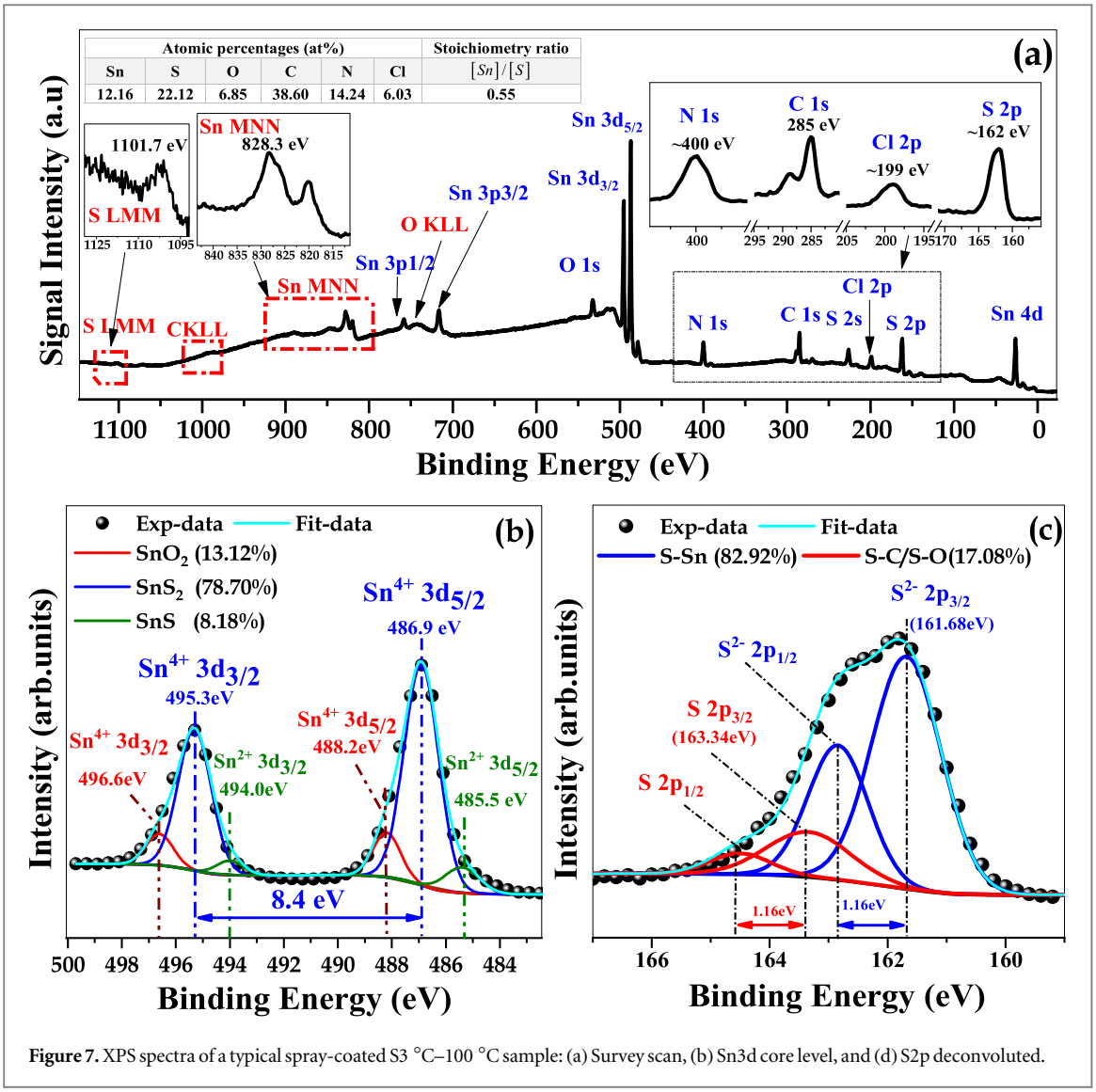

Figure 7. XPS spectra of a typical spray-coated S3 °C–100 °C sample: (a) Survey scan, (b) Sn3d core level, and (d) S2p deconvoluted.

Table 3. Electrical properties of spray-coated SnS_2 thin films.

Sample	σ (S/cm)	TEP (μV/K)	n (cm^{-3})	μ (cm^2/Vs)	Activation energy (meV)
S–60C	2.31×10^{-4}	−435	5.69×10^{21}	8×10^{-7}	40
S–80C	6.23×10^{-4}	−324	1.58×10^{21}	3.2×10^{-7}	50
S–100C	9.32×10^{-4}	−280	9.53×10^{20}	6.1×10^{-7}	90

with increasing solvent evaporation temperatures. Similar trend has been reported elsewhere for solution-processed SnS_2 thin films [21, 29, 36]. The low mobility might be a result of associated defects, impurities and grain boundary barriers in the ink-processed SnS_2 thin films. Higher value of n implies that density of defect states (situated near the conduction band) is also high. Hence, conduction of electrons through these defect states is highly probable.

The temperature dependent electrical conductivity of different types of spray-coated SnS_2 thin films have been measured above room temperature (300 to 400 K) as shown in figure 8. Electrical conductivity increases with increased temperature revealed semiconductor nature of the thin films.

Electrical conductivity also increases with increment in solvent evaporation temperature. It is well known that semiconductor thin films show thermally activated conduction (TAC) above room temperature. The film conductivity in spray-coated SnS_2 thin films above 300 K (until 380 K) is owing to band conduction. In the temperature range of 300 to 400 K, the plot of ln(σ) versus 1000/T, representing conduction by TAC, was found to be linear as shown in figure 9. The TAC is represented by equation (4) as:

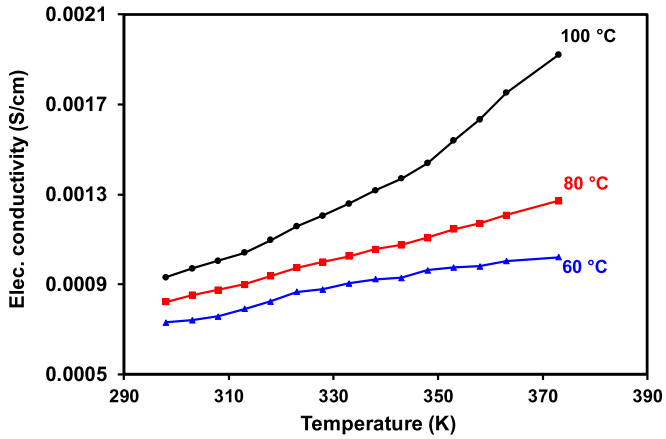

Figure 8. Temperature dependent electrical conductivity of spray-coated SnS_2 thin films.

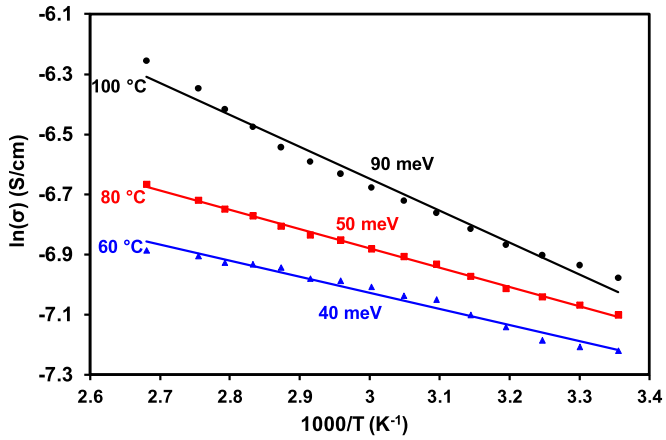

Figure 9. Temperature variation of electrical conductivity of spray-coated SnS_2 thin films.

$$\sigma = \sigma_0 \exp\left(-\frac{E_A}{k_b T}\right) \tag{4}$$

where,

σ_o is a constant,

E_A is the activation energy (eV) and

K_b is the Boltzmann constant (eV/K)

The activation energy estimated from the equation (4) was found to vary from 40 to 90 meV (table 3). Increment in activation energy with increasing solvent evaporation temperatures has been observed. These values of activation energies in SnS_2 films are an indication of defects. One of the major factors limiting the performance of optoelectronic devices is the occurrence of different types of defects including vacancies, antisites, and clusters which affects the charge transport mechanisms. In polycrystalline semiconductors, a large number of defects is presented due to the random atomic orientation, which results in the formation of trapping states. These trapping states are capable of trapping carriers and thereby immobilizing them. Similar results were elsewhere for SnS_2 thin films [37, 38].

Overall, it can be seen that the solvent evaporation temperatures have a profound effect on the physical properties of spray-coated SnS_2 films. However, films spray-coated at 100 °C show exceptional results including suitable band gap of 2.2 eV, low carrier concentration (10^{20} cm^{-3}) and compact grains as seen from SEM. The film quality (and ultimately the physical properties) of the spray-coated films depend upon many parameters; however, the most important is the flow rate and the other being substrate temperature. A molecular ink was synthesized with methanol having a boiling point of ~65 °C. The precursor films spray-coated above boiling point of methanol (S3 °C–100 °C) resulted in a smooth, homogeneous layer. In the spray coating process, the solvent evaporation and thermolysis stages are separate as shown in figure 1, thus imparting more control over processing and quality of film. The films are sprayed at low temperatures followed by solvent evaporation at high

thermolysis temperature. In general, the present investigation suggests that SnS_2 may be used as an alternative earth-abundant non-toxic Cd free buffer layer for Cu-based multicomponent chalcogenides thin film solar cells. Gedi *et al* [1] recently fabricated p-CIGS/n-SnS_2 solar cells and achieved ~5.1% efficiency suggesting that SnS_2 has potential as an alternative buffer.

4. Conclusions

n-type hexagonal SnS_2 thin films were spray-coated from transparent molecular ink synthesized with methanol. Spray-coated films were smooth, compact, and showed optimal bandgap from 2 to 2.2 eV perfectly suited as an alternative buffer material for solar PV devices. Structural and compositional analysis by x-ray photoelectron and Raman spectroscopy confirmed the formation of hexagonal and stoichiometric SnS_2 thin films. The present results are useful to further develop SnS_2-based photovoltaic devices.

Acknowledgments

This work is a part of PRFU project N B00L02UN460120220001 supported by Belhadj Bouchaib Ain-Temouchenet University. The authors thank the Materials Research Centre (MRC), Malaviya National Institute of Technology (MNIT), Jaipur, India for providing measurement of Raman spectroscopy data.

Data availability statement

The data that support the findings of this study are available upon reasonable request from the authors.

ORCID iDs

Prashant R Ghediya https://orcid.org/0000-0001-9953-0471
Abdelkader Nebatti Ech-Chergui https://orcid.org/0000-0001-9118-1289
Sanat Kumar Mukherjee https://orcid.org/0000-0003-3538-1643
Jaymin Ray https://orcid.org/0000-0002-3593-9216

References

[1] Gedi S, Reddy V R M, Kotte T R R, Park C and Kim W K 2022 *Nanomaterials* **11** 1955
[2] Shinde P and Rout C S 2021 *Mater. Chem. Front.* **5** 516
[3] Chang R J, Tan H, Wang X, Porter B, Chen T, Sheng Y, Zhou Y, Huang H, Bhaskaran H and Warner J H 2018 *ACS Appl. Mater. Interfaces* **10** 13002
[4] Haghighi M, Minbashi M, Taghavinia N, Kim D-H, Mahdavi S M and Kordbacheh A A 2018 *Sol. Energy* **167** 165
[5] Ullah S, Bouich A, Ullah H, Mari B and Mollar M 2020 *Sol. Energy* **208** 637
[6] Aslan F, Arslan F, Tumbul A and Goktas A 2022 *Opt. Mater.* **127** 112270
[7] Suresh S and Uhl A R 2021 *Adv. Energy Mater.* **11** 2003743
[8] Hadke S, Huang M, Chen C, Tay Y F, Chen S, Tang J and Wong L 2021 *Chem. Rev.* **122** 10170
[9] Mooney J B and Radding S B 1982 *Ann. Rev. Mater. Sci.* **12** 81
[10] Chen H, Ding X, Pan X, Hayat T, Alsaedi A, Ding Y and Dai S 2018 *J. Power Sources* **402** 82
[11] Jaber A Y, Alamri S N and Aida M S 2012 *Jpn. J. Appl. Phys.* **51** 065801
[12] Amroun M N and Khadraoui M 2019 *Optik* **184** 16
[13] Panda S K, Antonakos A, Liarokapis E, Bhattacharya S and Chaudhuri S 2007 *Mater. Res. Bull.* **42** 576
[14] Amratisha K, Ponchai J, Kaewurai P, Ngat P P, Pinsuwan K, Kumnorkaew P, Ruankham P and Kanjanaboos P 2020 *Opt. Mater. Express* **10** 1497
[15] Chaudhuri T K and Tiwari D 2012 *Sol. Energy Mater. Sol. Cells* **101** 46
[16] Ghediya P R, Chaudhuri T K, Raj V, Chugh D, Vora K, Li L, Tan H H and Jagadish C 2018 *Mater. Sci. Semicond. Process.* **88** 120
[17] Ghediya P R, Joshi K K, Kasela P A, Chaudhuri T K and Kandoliya M 2019 *Mater. Res. Express* **6** 106419
[18] Kadari A S, Ech-Chergui A N, Mukherjee S K, Velasco L, Singh R K, Mohamedi M W, Akyildiz E, Zoukel A, Driss-Khodja K and Amrani B 2021 *Inorg. Chem. Commun.* **132** 108852
[19] Gedi S, Reddy V R M, Pejjai B, Park C, Jeon C-W and Kotte T R R 2017 *Ceram. Int.* **43** 3713
[20] Reddy T S and Kumar M C S 2016 *Ceram. Int.* **42** 12262
[21] Voznyi A, Kosyak V, Opanasyuk A, Tirkusova N, Grase L, Medvids A and Mezinskis G 2016 *Mater. Chem. Phys.* **173** 52
[22] Bokuniaeva A O and Vorokh A S 2019 *J. Phys. Conf. Ser.* **1410** 012057
[23] Mote V, Purushotham Y and Dole B J 2012 *Theor. Appl. Phys.* **6** 2
[24] Williamson G K and Smallman R E 1956 *Philos. Mag.* **1** 34
[25] Hadjiev V G, De D, Peng H B, Manongdo J and Guloy A M 2013 *Phys. Rev. B* **87** 104302
[26] Chandrasekhar H R, Humphreys R G, Zwick U and Cardona M 1977 *Phys. Rev. B* **15** 2177
[27] Katahama H 1983 *J. Phys. Chem. Solids* **44** 1081
[28] Tauc J and Menth A 1972 *J. Non-Cryst. Solids* **569** 8

[29] Jariwala A, Chaudhuri T K, Toshniwal A, Kheraj V, Patel B, Ray A and Mukhopadhyay I 2021 *Mater. Sci. Semicond. Process.* **131** 105852
[30] Chastain J and King R C Jr 1992 *Perkin-Elmer Corporation* **40** 221
[31] Choi M, William W, Hwang J, Yoon D and Kim J 2018 *J. Ind. Eng. Chem.* **59** 160
[32] Christ B V 2000 The Elements and Native Oxides (https://www.wiley.com/en-us/Handbook+of+Monochromatic+XPS+Spectra%3A+The+Elements+of+Native+Oxides-p-9780471492658)
[33] Li J, Hou X, Mao Y, Lai C and Yuan X 2020 *Energy Fuels* **34** 14995
[34] Boughrara L, Zaoui F, Sebba F Z, Bounaceur B and Kada S O 2022 *Int. J. Biol. Macromol.* **205** 651
[35] Ghediya P R, Chaudhuri T K and Vankhade D 2016 *J. Alloys Compd.* **685** 498
[36] Kawano K, Nakata R and Sumita M 1989 *J. Phys. D: Appl. Phys.* **22** 136
[37] Vijayakumar K, Sanjeeviraja C, Jayachandran M and Amalraj L 2011 *J Mater Sci: Mater Electron* **22** 929
[38] Patil S G and Tredgold R H 1971 *J. Phys. D: Appl. Phys.* **4** 718